Published in Supercond. Sci. Technol. 29 (2016) 085012 (8pp) doi:10.1088/0953-2048/29/8/085012

# Enhanced quench propagation in 2G-HTS coils co-wound with stainless steel or anodised aluminium tapes

A.B. Núñez-Chico, E. Martínez*, L.A. Angurel and R. Navarro

*Instituto de Ciencia de Materiales de Aragón, (CSIC – Universidad de Zaragoza), Zaragoza, Spain*

* E-mail: elenamar@unizar.es

**Keywords**: superconductor, quench, thermal stability, REBCO, coated conductor, pancake coils

**Abstract**:

Early quench detection and thermal stability of superconducting coils are of great relevance for practical applications. Magnets made with second generation high temperature superconducting (2G-HTS) tapes present low quench propagation velocities and therefore slow voltage development and high local temperature rises, which may cause irreversible damage. Since quench propagation depends on the anisotropy of the thermal conductivity, this may be used to achieve an improvement of the thermal stability and robustness of 2G-HTS coils. On pancake type coils, the thermal conductivity along the tapes (coil's azimuthal direction) is mostly fixed by the 2G-HTS tape characteristics, so that the reduction of anisotropy relies on the improvement of the radial thermal conductivity, which depends on the used materials between superconducting tapes, as well as on the winding and impregnation processes. In this contribution we have explored two possibilities for such anisotropy reduction: by using anodised aluminium or stainless steel tapes co-wound with the 2G-HTS tapes. For all the analysed coils, critical current distribution, minimum quench energy values and both tangential and radial quench propagation velocities at different temperatures and currents are reported and compared with the results of similar coils co-wound with polyimide (Kapton®) tapes.

## 1. Introduction

The thermal stability of superconducting systems based on second generation of high temperature superconducting (2G-HTS) tapes is a major issue in the design of reliable electric power applications working at medium or high magnetic fields and temperatures in the 30-50 K range, where the optimum overall investment costs and optimum energy efficiency may be attained. This is of even greater relevance for those devices working in vacuum and cooled only by thermal conduction.

2G-HTS conductors made from REBCO ($REBa_2Cu_3O_x$, RE= rare earth or Y elements) are coated conductors (CC) with high current carrying capabilities and are now commercially available [1-5]. These conductors are usually 4-12 mm wide tapes with metal substrates and external metal tapes (copper, brass or steel) or copper coatings to achieve the thermal stabilization and mechanical performances required for different applications.

The electrical insulation between adjacent turns in REBCO pancake coils is commonly obtained by co-winding the CC tapes with thin polymeric ribbons such as polyimide (Kapton®), aramid (Nomex®), polyester (Mylar®), etc. Furthermore, to support mechanical requirements at service and during cooling-down and warming-up cycles, epoxy resin impregnations are frequently added during coil fabrication. Such coils show low values of quench propagation velocity, $v_p$, of the order of a few cm/s, in the axial and azimuthal directions, and are much lower for the radial component [6-8]. The consequences are strong increases of local temperatures at the quench origin (hot spot) and slow rises of the overall coil voltage during the quench. Both factors complicate the quench detection and the implementation of the protection methods commonly used in low temperature superconductor (LTS) devices, which rely on the fast propagation of the normal zone and the appearance of large electrical resistance before reaching the irreversible local deterioration limits.

The greater the heat flux across superconducting tapes, insulating layers and epoxy impregnation, the larger the size of the coil's resistive normal zone. But this goal is not easy to achieve. For example, Sumption *et al* [6] manufactured a coil with a CC tape that was sputter-coated with ZnO to increase the thermal conductivity of the insulating material between turns, but did not achieve large improvements of the coil's radial propagation velocity, probably by the opposite combined effects of the coating and the coil´s epoxy impregnation between turns.

The co-winding of superconducting tapes with insulated or uninsulated stainless steel (SS) or copper ribbons has been proposed to enhance both radial thermal conductivity and mechanical strength of 2G-HTS coils as well as to provide parallel paths during runaway. Gupta *et al* [9] suggest the co-winding of CC tapes and uninsulated SS to improve quench protection of such coils working in the 20-80 K temperature range. Bascuñan *et al* [10] propose for a LTS/HTS NMR magnet cooled with liquid helium, the co-winding of BSSCO tapes with uninsulated stainless steel in the outer HTS coil, and the co-wounding of 2G-HTS tapes with copper insulated with polyester for the inner coil. Markiewicz *et al* [11] use SS tapes insulated in one side by alumina ($Al_2O_3$) sol-gel coating co-wound with 2G-HTS tapes for a high field 32 Tesla LTS/HTS magnet.

In this work we have explored two ways to improve the thermal stability of REBCO pancake coils that also reinforce the mechanical properties: co-winding the coated conductors with either anodised aluminium alloy tapes or uninsulated stainless steel tapes. In the first case, the presence of a thin alumina layer on both faces of the anodised Al tapes would provide good electrical insulation between layers. Besides, $Al_2O_3$ has good thermal conductivity at cryogenic temperatures [12], although it must be taken into account that thermal conductivity of aluminium anodic oxide layers is lower than the value of bulk, polycrystalline $Al_2O_3$, due to the porous structure and to the presence of oxygen defects and electrolyte anions in the oxide layer [13,14]. In the second case, co-winding with SS tapes would reinforce the coil mechanically, by enabling the use of higher tensions during winding that may avoid the development of shear stresses within the REBCO tapes that deteriorate the magnets upon thermal cycling. Certainly, ramped loss and longer transients during charge and discharge of the magnet is an issue to be taken into account in such non-insulated coils. Nevertheless, since stainless steel has low electrical conductivity, the time constants of such coils during charge-discharge are similar to insulated coils, whereas if the resistivity of the inserted metal is low, for example copper, the time constant is larger [15,16].

For all the analysed coils, minimum quench energy values and azimuthal and radial quench propagation velocities are reported and compared with those obtained in coils co-wound with Kapton.

## 2. Experimental

### 2.1 *REBCO coil fabrication and instrumentation*

Several pancake coils were fabricated using 2G–HTS tapes (4 mm wide and 0.1 mm thick) provided by Superpower Inc. and different configurations. The characteristics of the coils are given in Table 1. The used CC tapes have 50 μm thick Hastelloy substrate, ~0.2 μm buffer and ~1 μm REBCO layer, top and bottom ~ 2.0 μm layers of silver and are surrounded by a 20 μm thick copper coating for thermal stabilization. The coils have a 65-68 mm inner diameter, a number of turns between 10 and 20 and a height about 4 mm given by the 2G-HTS width.

**Table 1**. Characteristics of the analysed single pancake coils

| Coil name | SS10 | SS20 | AAl20 | K20-1 | K20-2 | Kh10 |
|---|---|---|---|---|---|---|
| Co-winding material | SS[(a)] | SS[(a)] | Anodised Al | Kapton® [(b)] | Kapton® [(b)] | Kapton® [(c)] |
| No. of REBCO turns | 10 | 20 | 20 | 20 | 20 | 10 |
| $Ø_{in}$ , $Ø_{out}$ (mm) | 65, 70 | 66, 73 | 68,76 | 65, 73 | 67, 73 | 65, 72 |
| $I_c$ (77 K) tape | 102 A | 102 A | 110 A | 94 A | 110 A | 101 A |
| $I_c$ (77 K) coil | 80 A | 65 A | 71 A | 58 A | 63 A | 65 A |

[(a)]Stainless steel 306L
[(b)]Kapton ribbon glued parallel to the CC tapes,
[(c)]Kapton helicoidally wrapped around the CC tapes.

Stainless steel tapes (~60 μm thick × 4 mm wide) derived by rolling commercial 306L rods, were co-wound with the 2G-HTS tapes in the SS10 and SS20 coils. The anodised aluminium tape (~90 μm × 3.5 mm) used in the AAl20 coil was derived by rolling a commercial wire of aluminium alloy 5356, followed by anodic oxidation. It must be noted that this was the minimum thickness achieved by our rolling machine without breaking the tape, which was different for each metal. The conditions for the anodising procedure were: constant voltage of 20 V during 30 minutes in a 2 vol.% dilution of commercial sulphuric acid (96% PA-ISO) at ~24 ºC. A 4.5 μm thick layer of $Al_2O_3$ was formed on both sides of the aluminium tape with this process. Finally, Kapton ribbons (25 μm × 4 mm, with a ~ 12.5 μm silicone adhesive) were used to manufacture K20-1, K20-2 and Kh10 coils, but whereas for coils K20-1 and K20-2 the Kapton was glued along one side of the CC tape, for Kh10 it was helicoidally wrapped around the coated conductor with an overlap of 30%.

SS10, K20-1 and Kh10 coils were impregnated turn to turn with the epoxy resin during winding, while SS20 and AAl20 were dry-wound and subsequently impregnated with Stycast 1266 in vacuum conditions. Since the coil K20-1 was damaged during quench measurements for measuring $v_p$, another coil (K20-2) was prepared but using the same impregnation method as SS20 and AAl20.

In all cases, a constant tensile force of 4 N was applied to the tape during winding. The CC tapes were wound with the substrate toward the inner part of the coil and the SS and anodized Al tapes are located over the face closer to the REBCO layer. To protect the first superconducting turns of the coils, two security turns of copper or steel were weld or glued with the first 2G-HTS turn. A PTFE former was used for the winding process and was removed before cooling down.

In order to measure the voltage and temperature distributions, the coils were instrumented with thin copper sheets, 75 μm thick and 2 mm wide, soldered to the tape during winding for voltage taps and thermocouple connections. In addition, a small strain gage 3 mm long, ~ 2 mm wide, 0.4 mm thick and 120 Ω of resistance, used as heater for quench experiments, was glued directly to the tape surface of the mid-turn using GE varnish.

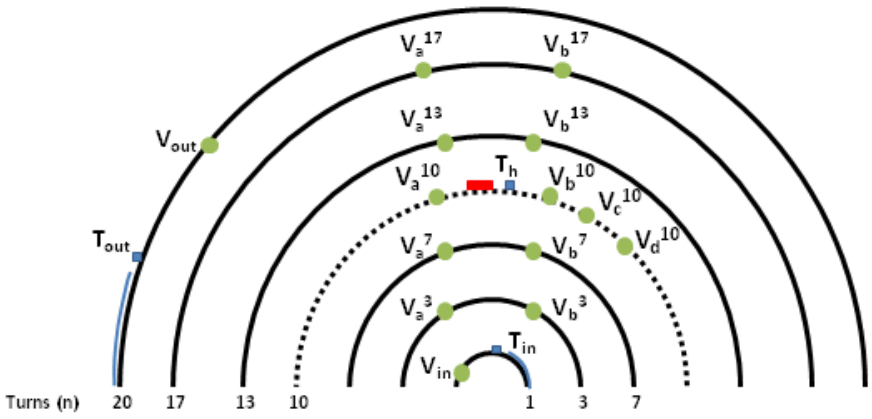


**Figure** 1. Schematic distribution of voltage taps and thermocouples inserted in the instrumented pancake coils SS20 and AAl20. The mid-turn (dotted line) allocates the heater, which is placed between $V_a^{10}$ and $V_b^{10}$ taps, and two additional taps named $V_c^{10}$ and $V_d^{10}$. $V_a^n$ and $V_b^n$ refer to taps of the *n*-turn. For clarity purposes, only the turns that allocate voltage taps have been drawn.

Figure 1 shows the positions of voltage taps used in coils SS20 and AAl20. The heater was glued on the REBCO side of the CC tape in the mid-turn of the coil ($n$=10) at equal distances of voltage taps $V_a^{10}$ and $V_b^{10}$. Along this turn two additional taps, $V_c^{10}$ and $V_d^{10}$, were disposed to estimate the quench propagation velocity along the tape in the coil's azimuthal direction, $v_{p,\varphi}$. Additional taps $V_a^n$ and $V_b^n$ were also located at inner and outer turns ($n$= 3, 7, 13 and 17) to detect the quench propagation velocity along the coil's radial

direction, $v_{p,r}$. Voltage taps $V_{in}$ and $V_{out}$ were placed close to the inner and outer current terminals, respectively, to measure the total coil voltage. Thermocouples $T_h$, $T_{in}$ and $T_{out}$ were soldered close to the heater and near both current terminals, respectively, for temperature control. Similar distributions of voltage taps were used in the other instrumented coils.

After winding, epoxy impregnation and final drying, the pancake coils were glued to an aluminium support disk by using an epoxy resin of good thermal conductivity (Stycast 2850 FT).

### 2.2 *Critical currents distribution within the coils*

Self-field critical currents values, $I_c$, of the starting tapes and of the coils were determined from the current *versus* voltage curves with the usual 1 μV/cm criterion. The $I_c$ values of the coils collected in table 1 were obtained by measuring the voltage between taps $V_{in}$ and $V_{out}$. The $I_c$(77K) values of different coil sections are shown in figure 2 for coils SS20, AAl20 and K20-2. The $I_c$ distribution inside the coils has been obtained by measuring the voltage drop in the different coil's sections (voltage measured between taps $V_a^i$ and $V_a^j$ was used to estimate $I_c$ in the coil's section between turns i and j). It is observed that the maximum of $I_c$ is obtained in the middle part of the coil, and the lowest in the inner turns, where self-field is minimum and maximum, respectively. The differences in the values measured in the different sections are lower than 10% of the $I_c$ of the coil. The observed behaviour is very similar for all manufactured coils.

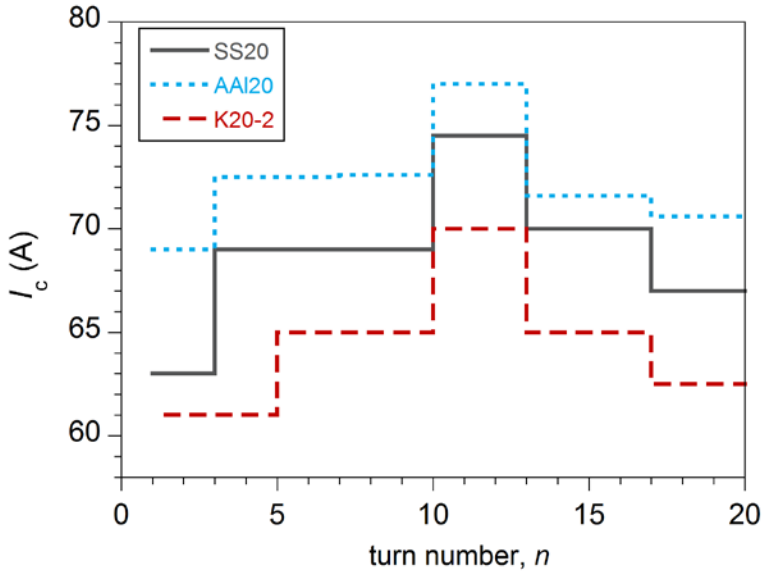


**Figure 2.** Distribution of critical currents $I_c$ measured in the different sections of pancake coils SS20, AAl20 and K20-2 immersed in liquid nitrogen at 77 K. The turns are numbered from inside $n$ = 1 to outside $n$ = 20.

### 2.3 *Thermal conductivity of stacks*

In order to estimate the radial thermal conductivity of the different coils, three stacks, named S-SS, S-AAl and S-K, were prepared using 10 to 15 CC tapes interleaved with the stainless steel, anodised aluminium alloy or Kapton, respectively, with the same distribution and dimensions used for the coils. An additional stack, S-Kh, was prepared with 10 CC tapes helicoidally wrapped with Kapton, to simulate the Kh10 coil configuration. All of them were impregnated with Stycast 1266 epoxy resin. The height of the stacks, $h$, ranges between 1.4 and 2.4 mm and their cross-sections, $A$, is 4 mm × 5-10 mm. To estimate the thermal conductivity across each stack, $k$, a heat power, $P$, is applied on one surface of the stack, and the temperature gradient $\Delta T$ is measured across the stack, so that $k = (P/\Delta T)\cdot(h/A)$. The results are shown in figure 3.

The thermal conductivities of stacks S-SS and S-AAl are very similar, $k$(77 K)=1.8 and 2.2 $Wm^{-1}K^{-1}$, respectively, which are about one order of magnitude higher than for the stacks made with Kapton, $k$(77K)= 0.25 and 0.14 $Wm^{-1}K^{-1}$ for S-K and S-Kh, respectively. As expected, the lowest $k$ values correspond to the S-Kh stack, due to the higher thickness of Kapton between superconducting layers. It is worth noting that Bai *et al* [17] have reported similar thermal conductivity values across stacks of CC tapes interleaved with non-insulated SS or with SS insulated by a sol-gel coating, $k$(77 K) ~ 1.6 and 0.6 $Wm^{-1}K^{-1}$, respectively.

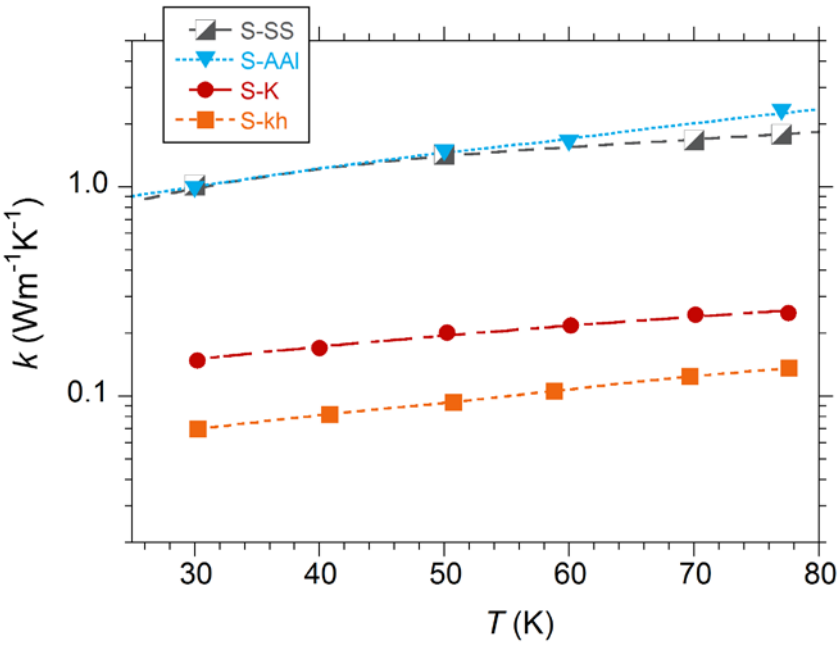


**Figure 3.** Measured thermal conductivity across different stacks of interleaved CC tapes and ribbons of SS (S-SS), anodised aluminium alloy (S-AAl) or Kapton (S-K), as a function of temperature. The results for a stack of CC tapes helicoidally wrapped with Kapton (S-Kh) are also shown.

2.4 *Experimental set-up for quench measurements*

For quench measurements, the pancake coils were in vacuum and cooled by thermal conduction. The aluminium support of the coils was mechanically attached to the second stage of the cryocooler cold finger. Apiezon® N was used between both surfaces to enhance the thermal contact. The operating temperature of the coil, $T_0$, was controlled with a Lakeshore temperature controller. Energy pulses, $Q_{ini}$, were deposited in the heater by passing rectangular current pulses of duration $t_p$ while a DC current, $I<I_c(T_0)$ was circulating in the coils. For all quench measurements the energy was controlled by changing $t_p$, while the voltage was fixed to the maximum value that stands the used heater without damaging, 14 V. The voltages between different taps and the temperatures measured by the thermocouples were recorded simultaneously using a data acquisition device. The heating pulse, data acquisition and the power supply used to energize the coils were controlled by a LabView program. In order to protect the coils during a quench two different methods were used:

*i)* Prior to the quench measurements the program sets the limit voltage in the power supply (2–3 V) and the elapsed time between the heat pulse and the switch-off of the power supply (2–4 s). This way, once the limit voltage is reached, further resistance increase in the coil will progressively diminish the current.

*ii)* The total voltage in the coil ($V_{in}$-$V_{out}$) is measured during the quench and when it reaches a given threshold value (2–2.5 V) the program switches the power off, so the current is set to zero.

Initially, quench measurements were carried out using the first method, but some coils were damaged during the experiments [7]. Subsequently, the second method was implemented, which was successful to prevent coil damage for all quench conditions presented in this paper.

## 3. Results and discussion

Figure 4 shows the evolution of the average electric field values in different regions of the coil SS20, which were derived from the measured voltages divided by the distance between taps. These measurements allow the estimation of the normal zone propagation velocities in both coil directions: the azimuthal (along the conductor) and radial (across the winding). They also give a rough estimation of the size of the minimum propagation zone, MPZ, which is the coil region where dissipation occurs at the moment when quench starts. This moment of quench triggering or initiation after a heat perturbation occurs when the coil voltage starts increasing irreversibly, which reflects the fact that the coil has entered

into an unstable regime ($t$ ~ 0.8 s for the quench displayed in figure 4, marked by an arrow).

To get an accurate value of MPZ, several voltage taps in all turns around the heater would be needed. But this larger instrumentation of coils could substantially affect the quench behaviour and was thus disregarded. By analysing the electric curves of the mid-turn where heater is placed ($n$=10 in this case), we conclude that MPZ along the conductor is shorter that 2 cm. On the other hand, we can also obtain a rough estimation of the size of MPZ across the winding by analysing the electric curves measured in the other turns. Thus, when quench triggers, electric field is zero in the outer turn ($n$=13) but not in the inner turn ($n$=7), which indicates that the normal zone does not grow symmetrically around the heater in the radial direction, but tends to be larger toward the inner region. This trend, observed in all analysed coils, is likely due to the uneven distribution of self-field critical currents within the coil that gives lower $I_c$ values for inner turns (see figure 2).

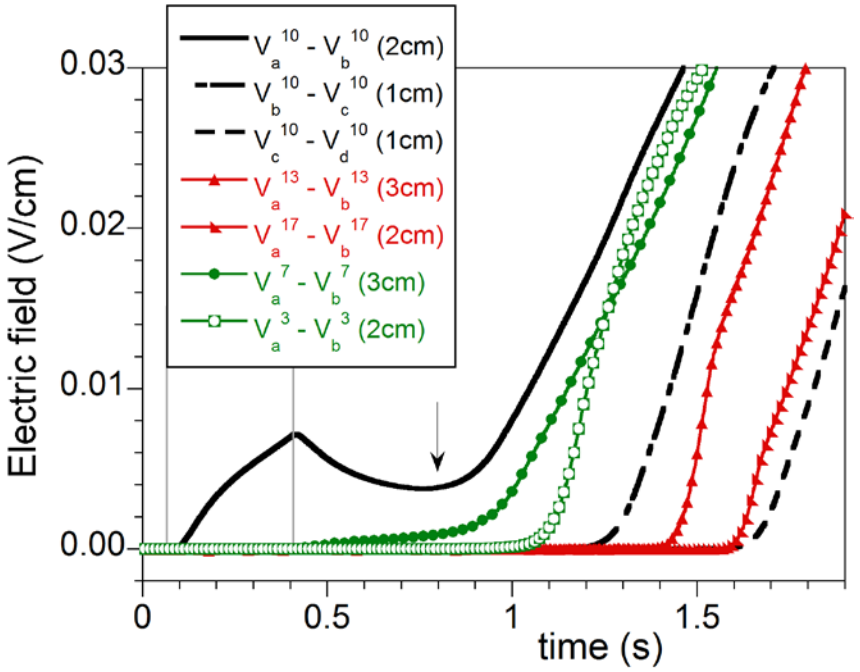


**Figure 4**. Time evolution of electric fields measured at different positions of coil SS20, for $I$ = 90 A~ 0.85·$I_c$ and 70 K, during a quench. Lines without symbols correspond to electric fields at the mid-turn ($n$= 10); Triangles refer to the outer turns ($n$=13 and 17) and circles to the inner turns ($n$=7 and 3). The distances between voltage taps are given in the label. Two grey vertical lines mark the start and the end of a 560 mJ heat pulse that triggers the quench and has a duration $t_p$=343 ms. The arrow points to the moment of quench triggering.

### *3.1 Quench propagation velocity* ($v_p$)

From the evolution of the electric fields generated between taps during a quench it is also possible to derive the radial ($v_{p,r}$) and azimuthal ($v_{p,\varphi}$) components of the quench propagation velocity, $v_p$. Since $v_p$ should be estimated outside the MPZ, the electric fields

measured in the inside turns ($n$=3 and 7) cannot be used to get $v_{p,r}$. Instead, $v_{p,r}$ was estimated from the radial distance between turns 13 and 17, divided by the time delay between electric field curves $V_a^{13}$- $V_b^{13}$ (3cm) and $V_a^{17}$- $V_b^{17}$ (2cm). Similarly, the elapse time measured between curves $V_b^{10}$- $V_c^{10}$ and $V_c^{10}$- $V_d^{10}$, with consecutive taps placed at equal distances of 1 cm, were used to estimate $v_{p,\varphi}$.

Figure 5(a) shows the quench propagation velocity components at 77 K for coils SS20, AAl20, K20 and Kh20. Moreover, since the critical current values of these coils are different, it is more significant to compare the $v_p$ values for the same coils at different operating temperatures to get the same critical current value. In figure 5(b) the results at 70 or 74 K depending on the coil and $I_c \sim 105$ A, have been represented.

The quench propagation velocity in the azimuthal direction, $v_{p,\varphi}$, is similar for all measured coils, and ranges from 14-40 mm/s for the different operating conditions. Moreover, it must be noted that $v_{p,\varphi}$, values are smaller than those measured for straight pieces of similar coated tapes, which range from 40-70 mm/s at 77 and 72 K and $I/I_c$ = 0.7-0.9 [18].

By contrast, propagation in the radial direction is strongly dependent on the coil architecture. The measured $v_{p,r}$ values increase by a factor of 3-4 when Kapton is substituted by steel and anodised aluminium. Therefore, the anisotropy of quench propagation, $v_{p,\varphi}/v_{p,r}$, decreases from 30, 35 for Kapton coils K20 and Kh20, respectively, to just 7, 9 for stainless steel and anodised aluminium coils, respectively. This behaviour is in agreement with the observed increase of the transverse thermal conductivity by the substitution of Kapton by SS or anodised Al (Fig. 3, section 2.3).

In the framework of a continuum medium model, where the impregnated coil is approached by an anisotropic effective medium with thermal conductivities $k_\varphi$ and $k_r$ along the azimuthal and radial directions, respectively, the anisotropy of quench propagation will be given by $(k_\varphi/ k_r)^{1/2}$ [7, 19, 20]. Assuming that $k_\varphi$ is dominated by the thermal conductivity of the coated tapes and $k_r$ values are given by those measured for their corresponding stacks (figure 3), the estimated anisotropy values would be ~ 40, 32, 12 and 10 for coils Kh20, K20, SS20 and AAl20, respectively. It must be noted that these are higher than the experimental values but in qualitative agreement despite its simplicity. A more accurate estimation should take into account the heterogeneous distribution of heat flow in the coated tapes, epoxy impregnation and materials used between turns, as well as

the thermal contact resistance between layers and the heat transfer from the winding to the cryocooler through the epoxy resin and support.

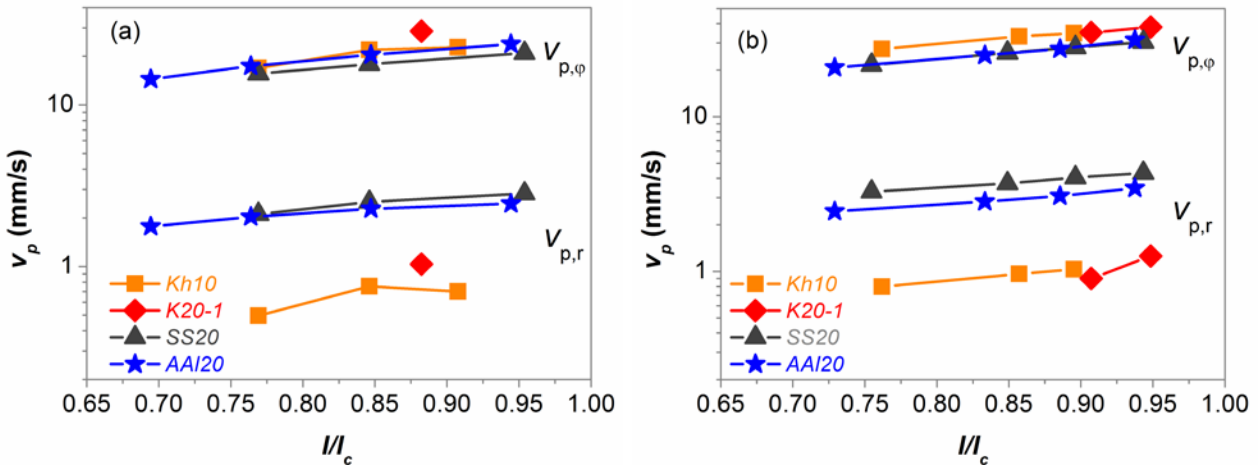


**Figure 5.** Quench propagation velocities in the coil's azimuthal ($v_{p,\varphi}$) and radial ($v_{p,r}$) directions for the analysed single pancake coils as a function of the reduced current, (a) at 77K; (b) at temperatures at which $I_c$~ 105 A ($T_0$ = 74 K for AAl20, and 70 K for the rest of the coils represented).

The fast increase of $V_{coil}(t)$ once the quench triggers is important to allow early quench detection and to design appropriate quench coil protection. It must be noted that the observed asymmetry of the MPZ in the radial direction also influences the voltage increase during the quench. This is more clearly observed in figure 6 where the overall coil voltage, $V_{coil}(t)$, is compared with the voltage measured in the inner ($V_{inner}$) and outer ($V_{outer}$) halves of coils SS20 and AAl20. With the tap distribution shown in figure 1, $V_{coil}(t)$ is measured between taps $V_{in}$ and $V_{out}$; $V_{inner}(t)$ between taps $V_{in}$ and $V^{10}{}_a$; and $V_{outer}(t)$ between taps $V^{10}{}_b$ and $V_{out}$. For the coil co-wound with stainless steel, SS20, there is a significant delay (~ 0.45 s) between $V_{inner}(t)$ and $V_{outer}(t)$. Nevertheless for the coil co-wound with anodised aluminium, seen in figure 6(b), this delay is significantly reduced to < 0.1 s. The insets in figure 6 show the same data in an enlarged scale to see in more detail the voltages when the quench triggers. It is seen that in both cases the voltage is not only originated in the mid-turn around the heater but also in the inner turns. Besides, it is seen that the minimum voltage that generates a quench is of the same order, but higher for SS20 than for AAl20 (24 mV and 18 mV, respectively, for the above conditions). Also note that $V_{inner}$ measured at the time of quench triggering is higher for SS20 than for AAl20, which suggests that MPZ in the radial direction is larger in the former.

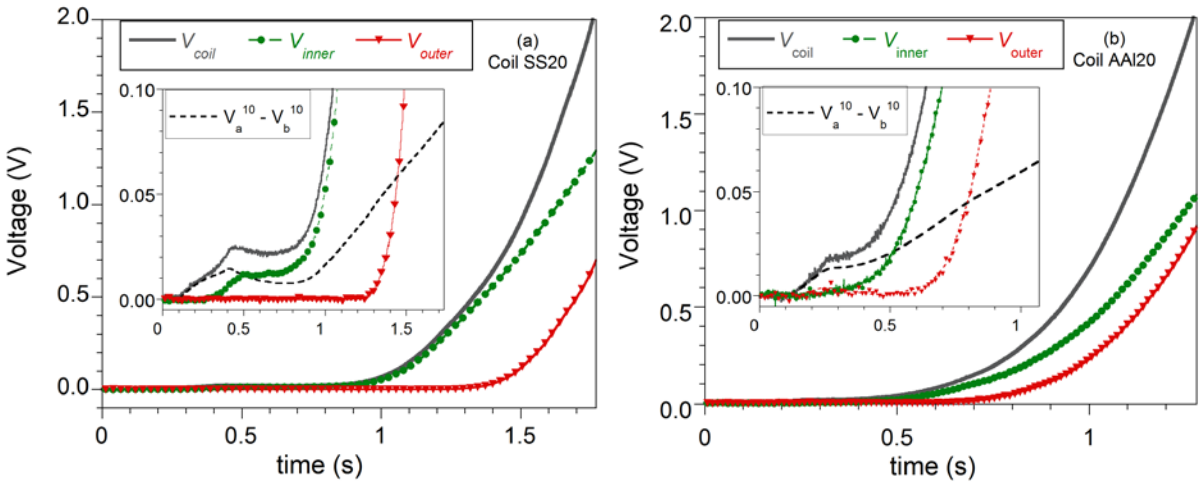


**Figure 6.** Time evolutions of the voltages during a quench at $I$ = 90 A~ 0.85·$I_c$ for (a) SS20 coil (70 K, $t_p$ = 340 ms), and (b) AAl20 (74 K, $t_p$ = 180 ms). Continuous lines are used for overall coil voltage, dashed lines for the voltage around the heater ($V_a^{10}$- $V_b^{10}$), and lines with circles and triangles for the voltage measured in the inner ($V_{inner}$) and outer ($V_{outer}$) halves of the coil, respectively. The insets show enlarged views of the quench initiation.

Figures 7(a) and 7(b) compare the voltage development $V_{coil}(t)$ during a quench in coils SS20, AAl20, K20-2, SS10 and Kh10. For clarity reasons not all curves are represented in both figures. As explained before, the comparison has been done for slightly different operating temperatures to get similar $I_c$ and $I/I_c$ conditions. Figure 7(a) compares the $V_{coil}(t)$ for coils made with anodised aluminium and Kapton. In this logarithmic representation, it is clearly seen that the threshold voltage needed to trigger the quench is similar for AAl20 and K20-2 (~ 20 mV), and much lower for Kh10 (~ 6.5 mV). This threshold voltage is directly related to the minimum quench energy value, as will be seen later. Besides, once the quench triggers, the voltage developed in the coil increases much faster when anodised aluminium is used between turns instead of Kapton. Particularly slow voltage rates are observed for the coil Kh10, because this configuration has the highest thermal insulation between turns.

Figure 7(b) shows the same data but in a linear representation. Coils AAl20 and SS20 have similar voltage increase rates after quench triggering, which is in agreement with the similar propagation velocities measured in both coils (Figure 5). Note that the shift between both voltage curves would mainly be due to the different triggering times ($t$ ~ 0.7 s and 0.5 s for SS20 and AAl20, respectively, for the shown measurements).

On the other hand, by comparing $V_{coil}(t)$ of both coils made with stainless steel tape, but different number of turns, SS20 and SS10, we observe almost identical behaviour up to $V_{coil}$~ 0.8 V, then the voltage increase rate is slightly slower for SS10 coil. By analysing the electric field curves measured in the different turns (similarly to those represented in Figure 4), we conclude that this effect is most likely due to the end effects in the radial

direction in SS10. This end effects are clearly more relevant in the coils co-wound with stainless steel than those with Kapton because of their higher $v_{p,r}$ values. The comparison between SS10 and Kh10 makes clear that the reason for the slow voltage increase during a quench in the latter should be attributed to the smaller radial quench propagation velocity measured in this coil.

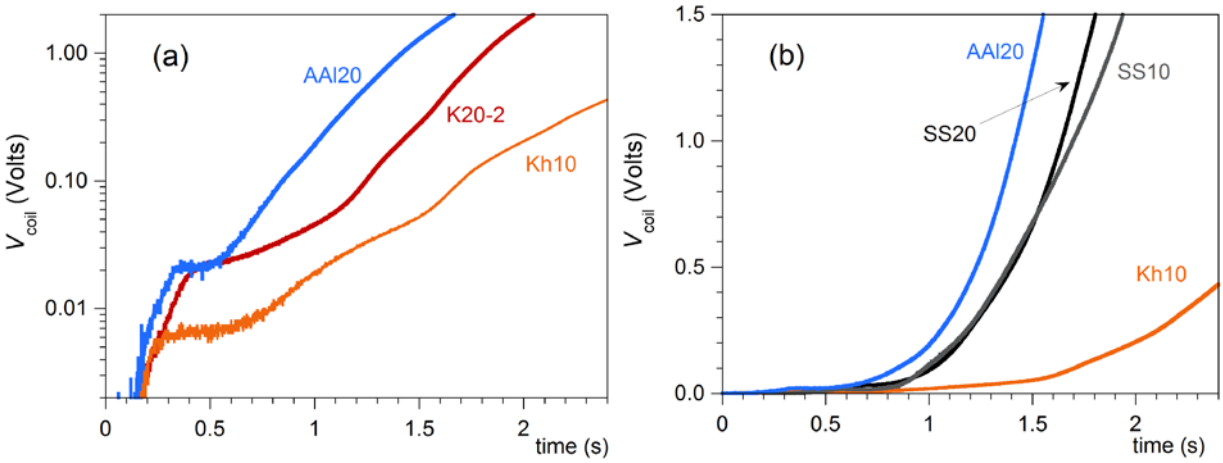


**Figure 7.** Time evolution of the overall coil voltages during a quench for $I$ = 80 A ($I$~ 0.75·$I_c$) for SS20, AAl20, K20-2, Kh10 and SS10 coils at $T$ = 70, 74, 71, 70 and 74 K, respectively; (a) in log scale, (b) in linear scale.

### *3.2 Minimum quench energy*

Figure 8 shows the minimum quench energy (MQE) in the measured coils at temperatures at which $I_c$ ~ 105 A in all of them. It must be noted that as before, the applied current has been divided by the critical current of the coil, not by the critical current value of the central section of the coil where the quench is developed.

Coils co-wound with stainless steel shows the highest MQE values, in agreement with already mentioned results of larger threshold voltages to trigger a quench for this coil. On the other hand, the lowest MQEs correspond to the coil Kh10, which is attributed to very low thermal conductivity between turns in this coil configuration of helicoidally wrapped Kapton over CC tapes. In all cases the measured MQEs in single pancake coils are considerably higher than those measured for similar CC tapes, which were 45 and 55 mJ at 77 and 72 K, respectively for $I/I_c$ =0.8 [18].

Besides, it must be noted that MQE values are expected to be higher for SS20 than for AAl20, since MPZ is larger in the former, as discussed previously (figure 6). A large MPZ of coils co-wound with SS would also explain the lower MQEs measured for SS10 coil compared to SS20, since MPZ extends to at least three turns towards the inner section of the coil, and therefore end effects could appear in SS10 coil.

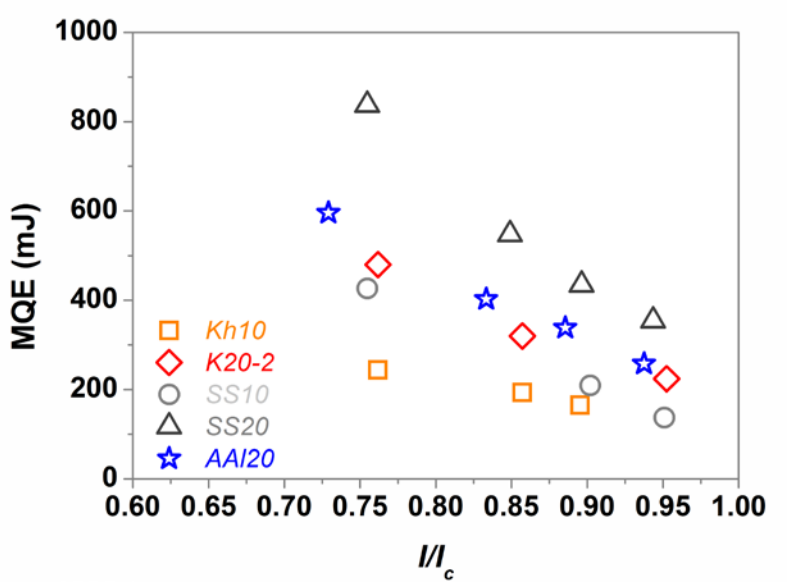


**Figure 8.** Minimum quench energy as a function of the reduced current, for the different analysed coils, at temperatures at which $I_c$~ 105 A ($T_0$ = 70, 71, 74, 70 and 74 K, for Kh10, K20-2, SS10, SS20 and AAl20, respectively).

## 4. Conclusions

The radial and azimuthal components of the quench propagation velocity have been measured in instrumented pancake 2G-HTS coils with different configurations. The effects of co-winding superconducting tapes with electric uninsulated stainless steel or anodised aluminium (insulated) tapes have been studied and the results compared with similar coils co-wound with Kapton.

The azimuthal quench propagation velocities (along the conductor direction) are very similar for all coils, showing a week dependence of the used inter-turn materials (SS, anodised Al or Kapton). However, the radial component increases by more than threefold if the coils are co-wound with stainless steel or anodised aluminium instead of Kapton.

It has been shown that the increase of the radial thermal conduction reduces the coil's thermal anisotropy, resulting in steeper overall coil voltage variations, larger quenched regions and faster propagation velocities, and thereby would facilitate the design of protection systems. Furthermore, it has been observed that quench does not develop symmetrically around the mid-turn where the heater is placed, but MPZ tends to be larger toward the inner turns, probably due to the self-field effects.

The highest MQEs correspond to the coil co-wound with stainless steel, and the lowest values to the coil made with a coated conductor insulated with helicoidally wrapped Kapton, which has the lowest thermal conductivity across the winding among all analysed

coils. For all measured configurations, MQE of single pancake coils are higher than those measured in single CC tapes.

The obtained results demonstrate that co-winding coated conductors with anodised aluminium or stainless steel tapes produces higher radial propagation velocities and steeper $V_{coil}(t)$ variations during quench propagation, which would be beneficial to get 2G-HTS coils more robust and easier to protect than when using Kapton as insulating material between turns.

## Acknowledgments

This work was supported by the Spanish Ministerio de Economía y Competitividad and the European FEDER Program (Projects MAT2011-22719 and ENE-2014-52105-R), and by the Gobierno de Aragón (research group T12). We also acknowledge the use of Servicio General de Apoyo a la Investigación- SAI, Universidad de Zaragoza.

## References


[1] SuperPower, Inc. http://superpower-inc.com

[2] SuperOx http://superox.ru/en/products/42-2G-HTS-tape

[3] American Superconductor http://amsc.com/solutions-products/hts_wire.html

[4] Fujikura Ltd, http://www.fujikura.com/solutions/superconductingwire/

[5] SuNam Co., Ltd www.i-sunam.com

[6] Sumption MD, Majoros M, Susner M, Lyons D, Peng X, Clark CF, Lawless WN and Collings EW 2010 *Supercond. Sci. Technol.* **23** 075004 (16pp)

[7] Nuñez-Chico AB, Martínez E, Angurel LA, Navarro R 2015 *IEEE Trans. Appl. Supercond.* **25** 6800604 (4pp)

[8] Song H, Gagnon K and Schwartz J 2010 *Supercond. Sci. Technol.* **23** 065021 (10pp)

[9] Gupta R et al 2011 *IEEE Trans. Appl. Supercond.* **21** 1884-1887

[10] Bascuñán J, Hahn S, Park DK, and Iwasa Y 2011 *IEEE Trans. Appl. Supercond.* **21** 2092-2095

[11] Markiewicz WD et al 2012 *IEEE Trans. Appl. Supercond.* **22** 4300704 (4pp)

[12] Ekin JW, "*Experimental Techniques for Low Temperature Measurements*". London, U.K.: Oxford Univ. Press, 2006.

[13] Ogden TR, Rathsam AD and Gilchrist JT 1987 *Materials Letters* **5** 84-87

[14] Lee J, Kim Y, Jung U and Chung W 2013 *Materials Chemistry and Physics* **141** 680-685

[15] Lee TS, Hwang YJ, Lee J, Lee WS, Kim J, Song SH, Ahn MC and Ko TK 2014 *Supercond. Sci. Technol.* **27** 065018 (8pp)

[16] Wang X, Hahn S, Kim Y, Bascuñán J, Voccio J, Lee H and Iwasa Y 2013 *Supercond. Sci. Technol.* **26** 035012 (6pp)

[17] Bai H, Markiewicz D, Lu J and Weijers HW 2013 *IEEE Trans. Appl. Supercond.* **23** 4600204 (4pp)

[18] Pelegrín J, Martínez E, Angurel LA, Xie Y-Y, and Selvamanickam V 2011 *IEEE Trans. Appl. Supercond.* **23** 3041 (4pp)

[19] Stenvall A, Korpela A, Mikkonen R and Grasso G 2006 *Supercond. Sci. Technol.* **19** 184-189

[20] Pelegrín J, Romano G, Martínez E, Angurel LA, Navarro R, Ferdeghini C, Brisigotti S, Grasso G and Nardelli D 2013 *Supercond. Sci. Technol.* **26** 045002